JOURNAL OF GEOPHYSICAL RESEARCH, VOL. 105, NO. C4, PAGES 8775–8788, APRIL 15, 2000

Large-scale drift of Arctic Sea ice retrieved from passive microwave satellite data

T. Martin[1] and E. Augstein

Alfred-Wegener-Intitute for Polar and Marine Research, Bremerhaven, Germany

Abstract. A method of determining the large-scale sea ice drift using 85.5 GHz Special Sensor Microwave Imager data are presented. A cross-correlation method is applied to sequential images of gridded data covering the entire Arctic. Individual correlation results are validated with ice velocities derived from buoy data. The satellite-derived mean drift values and the variabilities of the ice drift correspond closely with the buoy data. Similarly, time series of buoy data and associated satellite data are in good agreement even over large time periods. An example of a satellite-retrieved 3 day mean drift field demonstrates the potential of the method for providing large-scale ice circulation patterns. Mean drift fields of the winter periods 1987-1988 and 1992-1993 indicate a considerable interannual variability of the sea ice drift pattern in the Arctic Ocean. The Arctic region is divided into seven larger areas, and the area flux between these regions has been derived. The Kara Sea and the Laptev Sea show the largest area ice export with 0.02 and 0.015 $km^2\ s^{-1}$, respectively. The central Arctic export through Fram Strait amounts to 0.12 Sv during the winter of 1992-1993 with a maximum of 0.15 Sv in January.

1. Introduction

The motion of sea ice has important effects on the development and the budget of the ice cover of the polar oceans. The ice drift is permanently forced by the wind and ocean currents. The dynamical behavior of the ice cover is strongly affected by the internal stresses that arise from the mechanical strength of the ice cover. The ice cover is an insulating layer between the ocean and the atmosphere. Divergent and shear velocity fields result in cracks or leads. The opening in the ice creates areas of open water that significantly affect the air-ice-ocean interaction [*Stern et al.*, 1995; *Björk*, 1997]. During the ice growth the brine rejection and the fresh water flux associated with the ice motion represent a major driving mechanism of the global thermohaline circulation [*Aagaard et al.*, 1985]. Therefore observations of the sea ice velocity with a sufficient temporal and spatial resolution are required for both the Antarctic and Arctic. At present, data on ice motion are obtained from drifting buoys of the International Arctic Buoy Programme (IABP) [*Rigor and Heiberg*, 1997] and the International Programme for Antarctic Buoys (IPAB) [*Kottmeier et al.*, 1997]. The displacement of buoys on ice floes can be determined with a high spatial accuracy and temporal resolution of hours. However, the spatial distribution is generally rather coarse, so that buoy data provide only a highly restricted view of the temporal and spatial variability of the large-scale sea ice drift patterns [*Thorndike and Colony*, 1982; *Colony and Thorndike*, 1984, 1985; *Pfirman et al.*, 1997].

In contrast, data of satellite measurements cover the entire polar sea ice regions daily, so that the sea ice motion can be obtained from measuring the floe displacements in all parts of the area. In order to recognize the temporal displacement in the ice cover by satellite, special features such as leads, big floes, and rough or smooth ice must persist for several days. The sampling frequency and horizontal resolution of the employed radiometer must be well adjusted to the expected values of the sea ice drift velocities and to the temporal development of the recognized features. Several studies follow this intention of utilizing satellite data from advanced very high resolution radiometer (AVHRR) data or synthetic aperture radar (SAR). The high spatial resolution and the resulting large amount of data that have to be processed are reasons for applying these data more for investigation focused on regional processes, for example, to the Greenland Sea Current [*Martin and Wadhams*, 1999]. To investigate the drift field for the entire Arctic or Antarctic, more compact data sets are required. Passive microwave data with a pixel spacing of 12.5 km and a spatial resolution of 16×14 km have the potential to fill this gap.

[1]Now at Institute for Marine Research at the University of Kiel, Kiel, Germany.

Paper number 1999JC900270.
0148-0227/00/1999JC900270$09.00

In principle, microwave radar are able to provide high-quality sea ice drift data, but up to now the temporal and spatial coverage by these instruments has not been satisfactory, while the radiometer of the Special Sensor Microwave Imager (SSM/I) has been operating successfully for 10 years already. In the meantime the techniques for the retrieval of ice motion from passive microwave data have been considerably improved so that quite comprehensive information on the ice motion can now be provided [*Agnew and Le,* 1996; *Emery et al.,* 1997; *Kwock et al.,* 1998].

The Arctic sea ice cover varies annually in its area extent from a maximum of 14.8×10^6 km^2 in March to half this value in September [*Barry et al.,* 1993]. In September, at the end of the melting season the remaining ice is defined as multiyear ice. During the cold season the ice area increases and reaches its maximum between February and March. The sea ice concentration in the central Arctic amounts to nearly 100% during winter time. The high-frequency channels of the SSM/I are able to discriminate between first-year/new ice and multiyear ice, so that certain structures can be detected. The lower salinity of multiyear ice has been identified as the primary cause of the difference in radiometric signatures between multiyear ice and first-year ice [*Hallikainen and Winebrenner,* 1992]. The emissivity of sea ice in the SSM/I channels at 37 and 85.5 GHz shows a strong dependence on the ice development, which may also correlate with ice age. Because of differences in the history and the formation of ice, the electromagnetic properties of the multiyear ice cover are not homogeneous, differing primarily with respect to volume scattering. Several earlier studies employed these characteristics in their classification schemes [*Cavalieri et al.,* 1984; *Gloersen and Cavalieri,* 1986; *Comiso,* 1986]. *Comiso* [1990] outlined the difficulties involved in the derivation of the multiyear ice fraction from the radiometer signal. However, the internal structure of the brightness temperature field is stable enough so that such features can be employed to mark individual ice bodies during periods of days to even a month. Therefore automated detection procedures, which were originally developed for high-resolution optical or radar data [*Ninnis et al.,* 1986; *Emery et al.,* 1991; *Fily and Rothrock,* 1987; *Kwok et al.,* 1990], may also be applied to passive microwave signals.

Simple animations of SSM/I brightness temperature (TB) scenes (85.5 GHz channel) over the Northern Hemisphere sea ice cover provide a first impression of large-scale sea ice dynamics. Current studies attempt to derive the ice drift from the SSM/I data field. *Agnew and Le* [1996] show that images of the 85.5 GHz SSM/I brightness temperature contain a temporal displacement of features that are related to the drift buoy motion in the Arctic during wintertime. In a more detailed analysis, *Emery et al.* [1997] retrieved the mean annual sea ice drift for both hemispheres with an RMS error of 0.06 m s^{-1} for a combination of buoy data with SSM/I drift data. *Kwok et al.* [1998] have shown in a comparison with buoy data and SAR drift fields that the SSM/I drift retrieve for the large-scale Arctic ice drift also agrees very well. In this paper we will derive the large-scale velocity field of the Arctic sea ice during the winter period of 1987-1988, which was the first complete winter period of the SSM/I, compare this to the much more different winter, which was found in 1992-1993, and apply these results to derive statements concerning the transport budget of the Arctic ice cover.

2. SSM/I Data

The SSM/I has been operating since 1987 as part of the U.S. Defense Meteorological Satellite Program (DMSP) on a Sun synchronous, near-polar, and near-circular orbit. The radiometer measures the thermal emission at frequencies of 19.35, 22.23, 37.0, and 85.5 GHz. Except for 22.23 GHz all channels distinguish the horizontal and vertical polarization of the radiation. The sensor samples every 12.5 km along track at 85.5 GHz, and every 25.0 km along track at lower frequencies. The footprint size varies with frequency (19.3 GHz: 70×45 km; 22.2 GHz: 60×40 km; 37.0 GHz: 38×30 km; and 85.5 GHz: 16×14 km). The swath width of 1394 km provides a global coverage between latitudes 87°N and 87°S. Comprehensive details on the SSM/I system are given by *Hollinger et al.* [1987]. In this study we employ the daily 85.5 GHz SSM/I brightness temperature data provided by *National Snow and Ice Data Center (NSIDC)* [1996]. The data are mapped onto a 12.5 km Northern Hemisphere grid by converting the SSM/I geodetic latitude and longitude for the center of each measurement into SSM/I map grid coordinates. For each grid cell, brightness temperatures observed over a 24 hour period (midnight to midnight Greenwich mean time (UT)) are combined to obtain an average brightness temperature. If no observations fall within a grid cell, the average brightness temperature is assigned a corresponding label. The geolocation error is less than 1 pixel. The brightness temperature grids are precise to 0.1 Kelvin [*NSIDC,* 1996].

The radiation measured at the satellite results from the emission at the Earth surface and various effects along the transfer path through the atmosphere. A successful retrieval of the sea ice drift from brightness temperature data requires stable radiation characteristics of the sea ice over a several day period and a negligible influence of the atmospheric conditions. Most of the sea ice classification algorithms assume a totally transparent atmosphere in the microwave band. This leads to reliable results in conditions in moderate cloud and water vapor conditions [*Maslanik,* 1992]. *Gloersen and Cavalieri* [1986] as well as *Walters et al.* [1987] have suggested methods to eliminate situations with critical weather events. The influence of atmospheric processes

on the microwave signal increases with increasing frequency. Therefore the 85.5 GHz measurements have not been commonly used for sea ice detection.

In the 85.5 GHz spectral range the emissivity of the ice decreases with age, whereas liquid water fractions in the ice and in the snow layer increase the emissivity. During the winter the Arctic sea ice depicts in the 85 GHz channels a clear structured image where the main spatial characteristics could be detected for weeks. These conditions change dramatically in the springtime. The seasonal warming begins in April where the moisture content of the snowpack increases. The summer melt of the Arctic sea ice starts in May. During this period the spatial distribution of the radiative characteristics of the ice changes rapidly [*Eppler et al.*, 1992]. Under these conditions, simple drift algorithms are not able to distinguish between the internal changes in the ice layer and the spatial changes caused by ice motion.

Therefore we restrict our investigation in the Arctic for the period from October to March, when low temperatures are dominant, corresponding to atmospheric conditions of low water vapor and low cloud water contents [*Vowinckel and Orvig*, 1970]. During these periods the emission from the ice surface dominates the radiation signal received by the satellite.

3. Derivation of Ice Velocity Fields

3.1. Method of Drift Velocity Determination

Algorithms for the determination of ice motion by tracking common features in pairs of sequential satellite images have been developed and applied to data from different sensor types by several authors. All of these algorithms detect the displacement of features in pairs of images. For instance, *Ninnis et al.* [1986], *Emery et al.* [1991], or *Fily and Rothrock* [1987] have proposed methods based on the maximum of local cross correlations applied to SAR and AVHRR images. These techniques are insensitive to the rotation of single ice floes and to deformation that occurs in the ice cover leading to pressure ridge development. *Kamachi* [1989] investigate procedures to derive velocities from rotational flow fields from sequential images. *Kwok et al.* [1990] have investigated an improved tracking algorithm for SAR images that involves special feature matching routines for the sea ice remote sensing.

All techniques mentioned so far can only detect the displacement of features with large spatial dimensions compared to the horizontal pixel resolution. The horizontal resolution of the SSM/I data did not allow the tracking of single ice floes. The features in an SSM/I image are determined by larger areas with the same structure or a similar age, which are evidently visible in the brightness temperature images and smaller structures with horizontal diameters of several pixels (12.5 km per pixel) that are the result of new ice formation after periods of local divergence. The displacement of these structures in the images could be explained by a simple translation. The rotation in the ice field on a timescale of some days is negligible. Consequently, we have employed the simple area cross-correlation technique, which has already produced good results for AVHRR data in the Greenland Sea [*Martin and Lemke*, 1995; *Martin and Wadhams*, 1999].

Although the 85.5 GHz channel has the highest horizontal resolution of the SSM/I system, it can only detect relatively large scale structures of the sea ice cover (larger than a single ice flow). This spatial restriction of the sensor has to be taken into account for adapting the algorithm. During October to March the major number of buoy drift measurements are located in the interval <0.3 m s^{-1}, and in addition, a sizable number of drift measurements are even less than 0.01 m s^{-1} [*Lemke et al.*, 1997]. An optimal drift algorithm would retrieve the total spectrum of observed drift values. Here the applied method is limited because of the lower spatial resolution of the 85 GHz satellite data. However, we would propose to retrieve drift values that are <0.01 m s^{-1} using our method. If we propose to retrieve a minimal velocity of 0.01 m s^{-1} in the drift velocity for a single calculation, at a grid resolution of 12.5 km a time difference of ~347 hours (14 days) is necessary. Unfortunately, the correlation in pairs of images is too low after a period of 14 days, and our applied correlation scheme provides no utilizable results after this period. Since we are interested in ice drift retrievals covering temporal averaging periods as small as possible and in climatological drift fields, a correlation period of 72 hours was chosen for a box size of 87.5×87.5 km (7×7 Pixel) with a maximum search radius of 100 km (this is equivalent to a maximum drift velocity of $v_{\max} = 0.386$ m s^{-1}). The drift calculations were masked by the ice extent as retrieved by the NASA Team algorithm [*Cavalieri et al.*, 1984; *Gloersen and Cavalieri*, 1986; *NSIDC*, 1996]. To extend the retrieval interval of the estimated drift field, area averages were performed. Such a box contains $N = 25$ independent estimates of the ice drift. Therefore the variance of the estimated mean value decreases with $\sim 1/\sqrt{N}$ to $<\Delta v = 0.01$ m s^{-1}. Consequently, each drift vector in Figure 1 represents an area of 375×375 km. Through several sensitivity calculations we discovered that errors in the determination of the drift vectors occur mostly as a result of atmospheric effects or because of correlation of noncorresponding features on the ice cover. Unfortunately, we could not quantify the the errors from atmospheric effects. However, these uncertainties of the algorithm can be eliminated by on a number of tests. The test routines exclude vectors resulting from a small correlation or vectors with large differences in the direction or velocity with respect to the surrounding vector field.

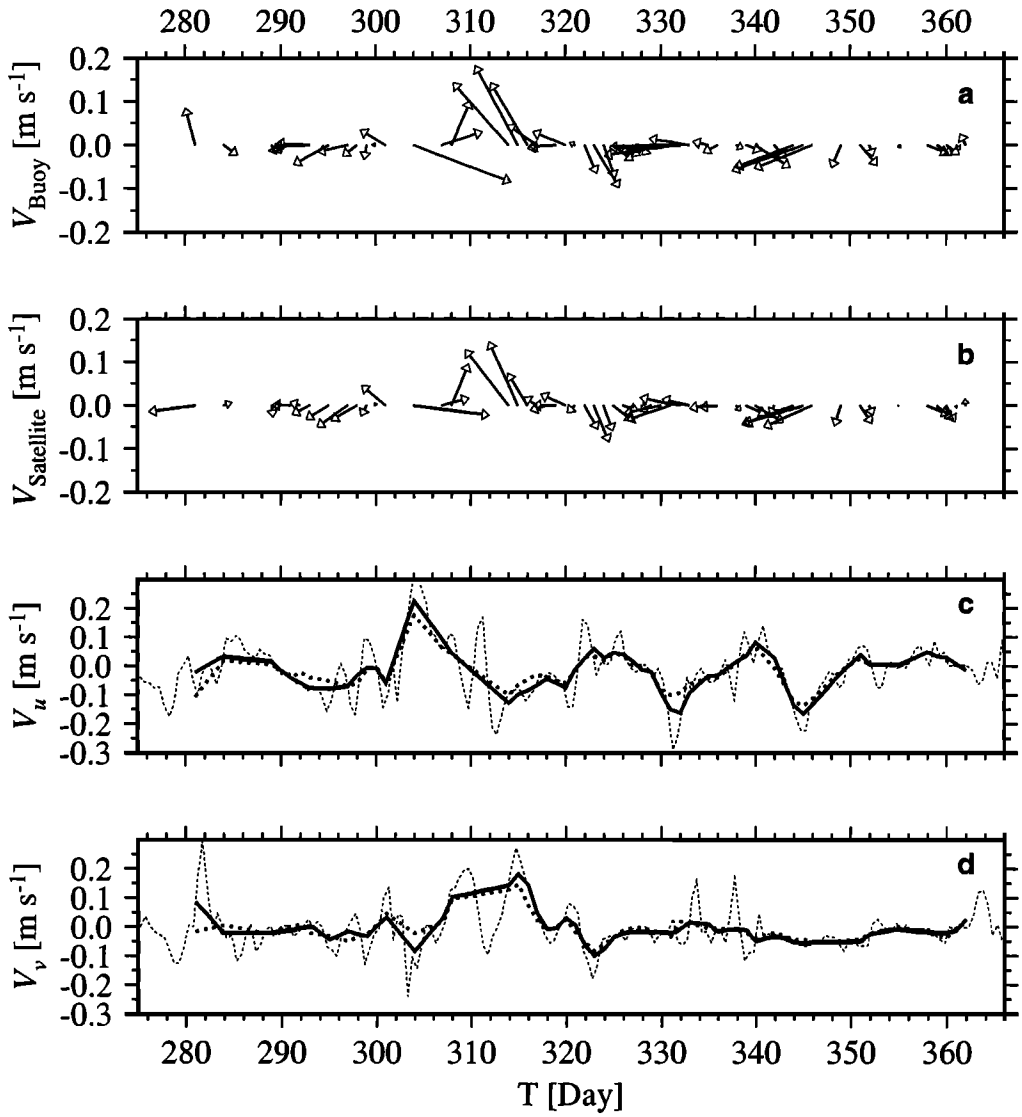

Figure 1. Time series of the ice drift from October 1 to December 31, 1992, for buoy number 11252 located approximately at 71.5°N, 133°W: (a) drift vector derived from buoy data, (b) drift vector derived from Special Sensor Microwave Imager (SSM/I) data, (c) zonal velocity component, and (d) meridional velocity component. The dashed lines indicate the 12 hour mean buoy data; the solid lines indicate the 3 day mean buoy data; and the dotted lines indicate the 3 day mean SSM/I data.

3.2. Validation of Ice Drift Retrieval

For the validation of our retrieval technique we relied on an independent data set of the large-scale ice drift in the Arctic. The most common drift data are provided by the IABP [*Rigor and Heiberg,* 1997], which has operated since 1979. The IABP supports a network of automatic buoys monitoring the synoptic-scale fields of pressure, temperature, and ice motion throughout the Arctic Basin. The ice drift is calculated from the temporal displacement of the buoy position, which has mostly localization errors smaller than 350 m. Thus the buoys provide the in situ ice motion for a larger number of locations at a high frequency.

The ice velocity retrieved from the remote sensing data of ice displacement represent a temporal and spatial mean. In contrast, the buoys measure the velocity of single ice floes [*Colony and Thorndike,* 1985]. Both data sets are highly scale-dependent. Therefore comparisons are limited to cases in which the motion of single ice floes represents the large-scale ice drift. Such conditions prevail in the central Arctic during periods of high ice concentration, when the motion field of single ice floes is strongly determined by the pack ice motion forced by the large-scale surface wind field and the ocean currents.

To test the remote sensing retrieval technique the 12 hourly buoy position data provided by the IABP were used to calculate 3 day average buoy drift velocities. Then each buoy drift value was related to the nearest SSM/I drift field entry. Figures 1 and 2 provide two

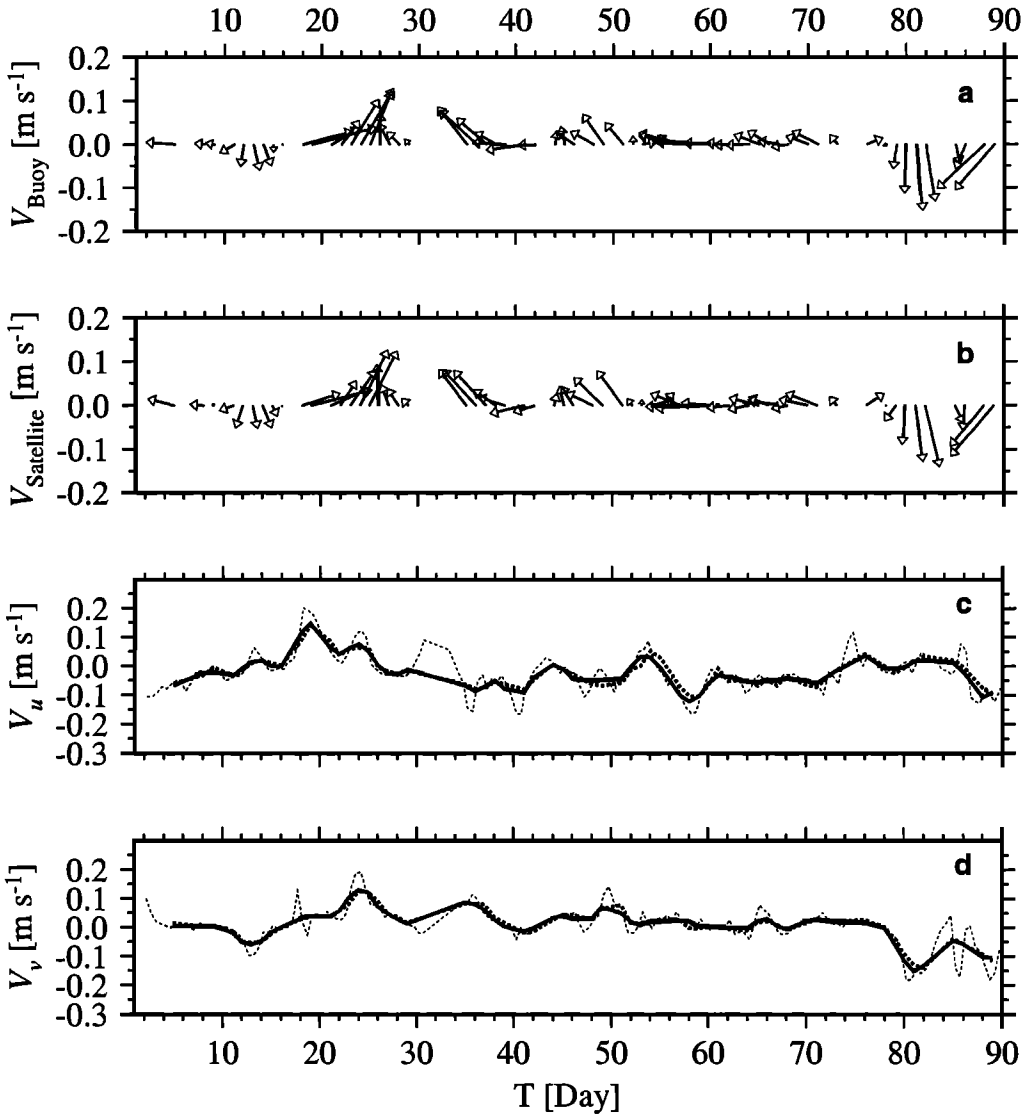

Figure 2. Same as Figure 1 but for January to March 1993 for buoy number 9360 located appproximately at 85.5°N, 113°E.

time series of corresponding satellite and buoy velocities with a correlation coefficient better than $r = 0.93$ in both cases. These selected examples demonstrate a very good correspondence during periods of low variability as well as during strong drift events. From these and other similar results, retrieving the large-scale sea ice drift from SSM/I measurements on a temporal averaging interval over 72 hours appears promising, while the short-term variance as indicated by the 12 hourly mean buoy drift cannot be detected by the satellite retrieval technique.

Statistics of 1941 single-drift measurements of 38 buoys between October and December 1992 and of 1630 drift measurements of 41 buoys between January and March 1993 together with similar values of satellite-based velocities are displayed in Tables 1 and 2. The data cover the entire Arctic Basin. Not only do the buoy displacements and the SSM/I drift values agree in speed (mean difference between buoy and satellite is

Table 1. Mean Components of the Drift Velocity Components $\bar{u}$ and $\bar{v}$ and the Related Variances σ_u and σ_v As Well As the Correlation Coefficient r Between Both Data Sets for October-December 1992.

	$\bar{u}$, m s^{-1}	σ_u	$\bar{v}$, m s^{-1}	σ_v
Buoy drift	-0.0138	0.0028	-0.0022	0.0030
SSM/I drift	-0.0132	0.0028	-0.0016	0.0030
Buoy - SSM/I	-0.0007	0.0008	-0.0007	0.0007
r	0.868		0.88	

SSM/I is Special Sensor Microwave Imager.

Table 2. Same as Table 1 but for January-March 1995

	$\bar{u}$, m s^{-1}	σ_u	$\bar{v}$, m s^{-1}	σ_v
Buoy drift	-0.0094	0.0029	-0.0007	0.0036
SSM/I drift	-0.0087	0.0027	0.0018	0.0032
Buoy - SSM/I	-0.0008	0.0006	-0.0019	0.0005
r	0.897		0.921	

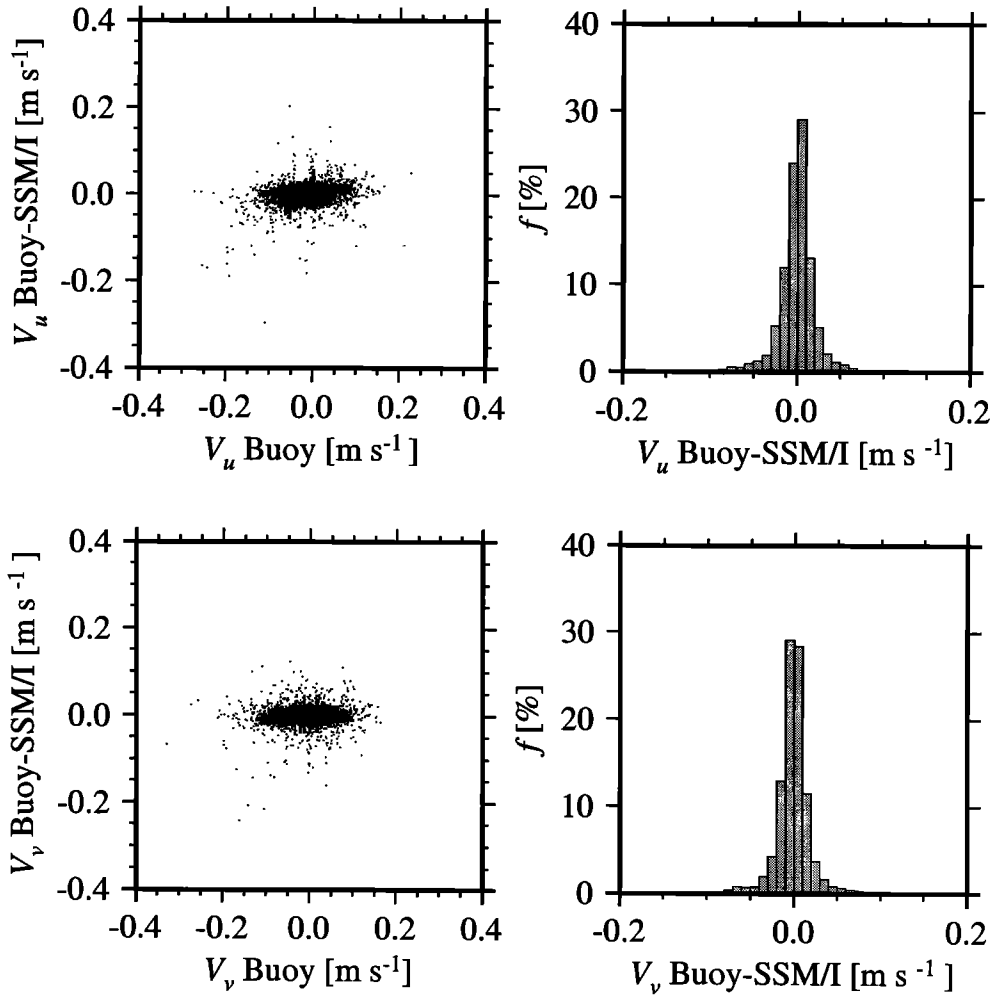

Figure 3. Distribution of the deviation in the velocity components between satellite data and buoy data during the winter 1992-1993; (top) deviation in the zonal velocity component, (bottom) deviation in the meridional velocity component, (left) scatter diagram of the difference between buoy data and satellite data against the absolute velocity, and (right) histogram of the difference between buoy data and satellite data.

0.001 m s^{-1}) and direction, but also, the variances of both data sets compare satisfactorily. Deviations between the SSM/I and buoy data for each velocity component are shown in Figure 3. These graphs show that both data sets differ stochastically but not systematically. These facts and the high mean correlation coefficient (see Table 1) suggest a high confidence in the SSM/I-derived velocity fields.

Consequently, the velocity field in Figure 4, which comprises measurements and SSM/I drift data, represents a reliable picture for the entire Arctic Ocean. With the aid of satellite data an increased cover of the ice drift is obtained. Features such as the cyclonic drift pattern in the Laptev Sea and the distinct divergence of the flow in the northern sector of the East Siberian Sea become clear.

4. Ice Drift Velocities Derived for Arctic Sea Ice

The actual drift calculations cover the periods from October 1987 to March 1988 and from October 1992 to March 1993; the averages are displayed in Figure 5. Significant differences in the drift pattern are evident for the two winter seasons. In 1987-1988 the Beaufort Gyre is well developed, and the ice flow from the East Siberian Sea is diverted into this circulation system. In contrast, the Beaufort Gyre is rather weak in 1992-1993, and ice from the East Siberian Sea joins the Transpolar drift together with the flow from the Laptev Sea. In both cases the drift in the Fram Strait region and the the East Greenland Current are well pronounced. The velocity histograms of both cases indicate nearly loga-

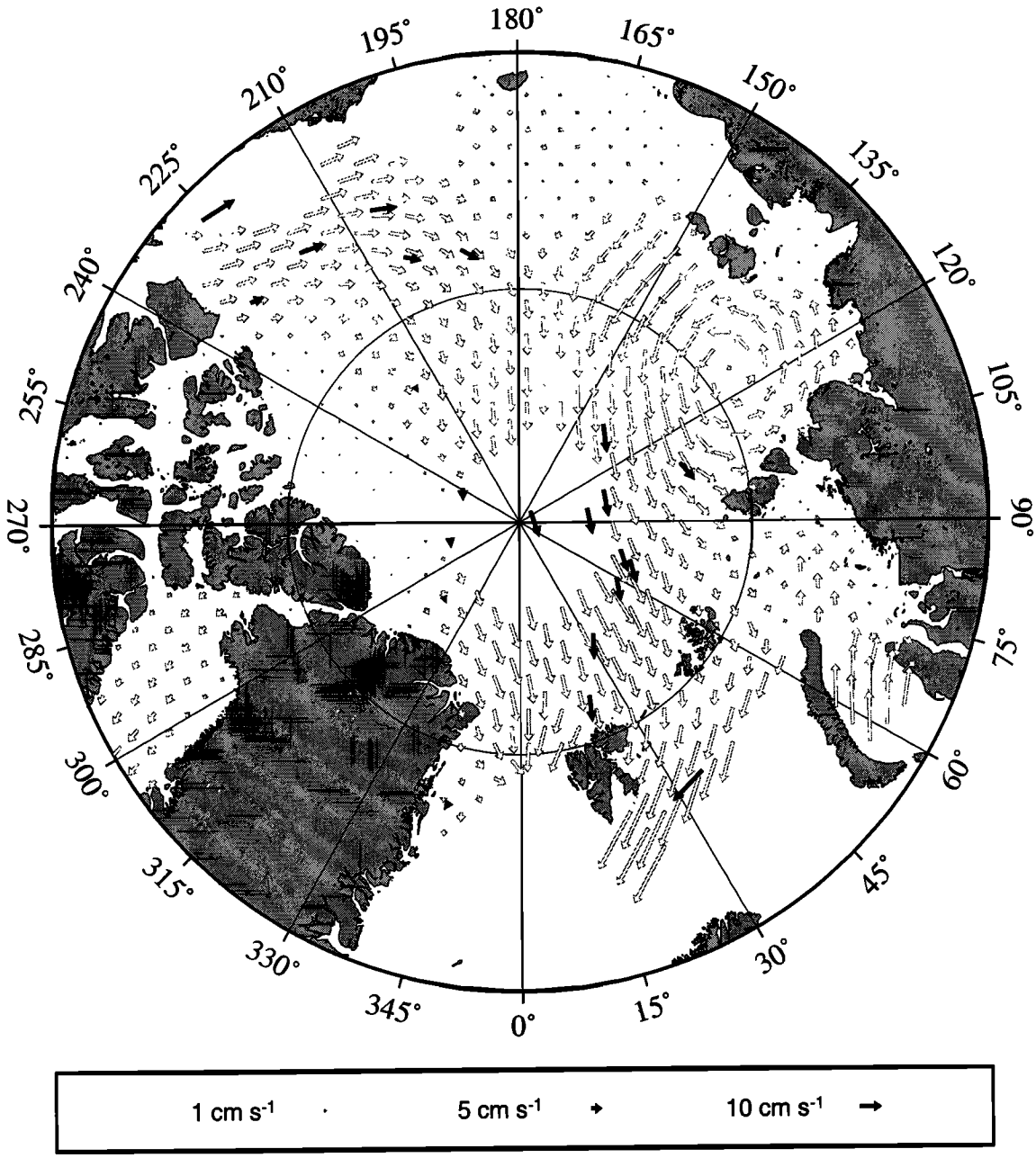

Figure 4. Arctic ice drift between Februray 25 and 28, 1993, derived from SSM/I data (shaded) and from buoy data (solid).

rithmic distributions between zero and 1.5 m s^{-1} (Figure 6). There are strong differences in the ice drifts, in the Kara and Barents Seas during the above mentioned two winter seasons (see Figures 5 and 6). The ice drift in the Kara Sea is directed northeast with values up to 0.05 m s^{-1} in winter 1987-1988. When the ice reaches the adjacent regions of the Barents Sea and the central Arctic Ocean the drift velocities decrease to much smaller values. This leads to a convergence ice drift between Franz Josef Land and Severnaya Zemlya. In contrast to this, in winter 1992-1993 the drift leads to a well-pronounced ice current from the Kara Sea into the Barents Sea.

Earlier studies of *Colony and Thorndike* [1984] and *Serreze et al.* [1989] have shown that the mean atmospheric surface pressure field and thus the geostrophic surface wind determine most of the mean ice circulation. Only in the Fram Strait region is the strong ocean current a prominent additional factor for the ice drift. *Power and Mysak* [1992] have pointed out that besides

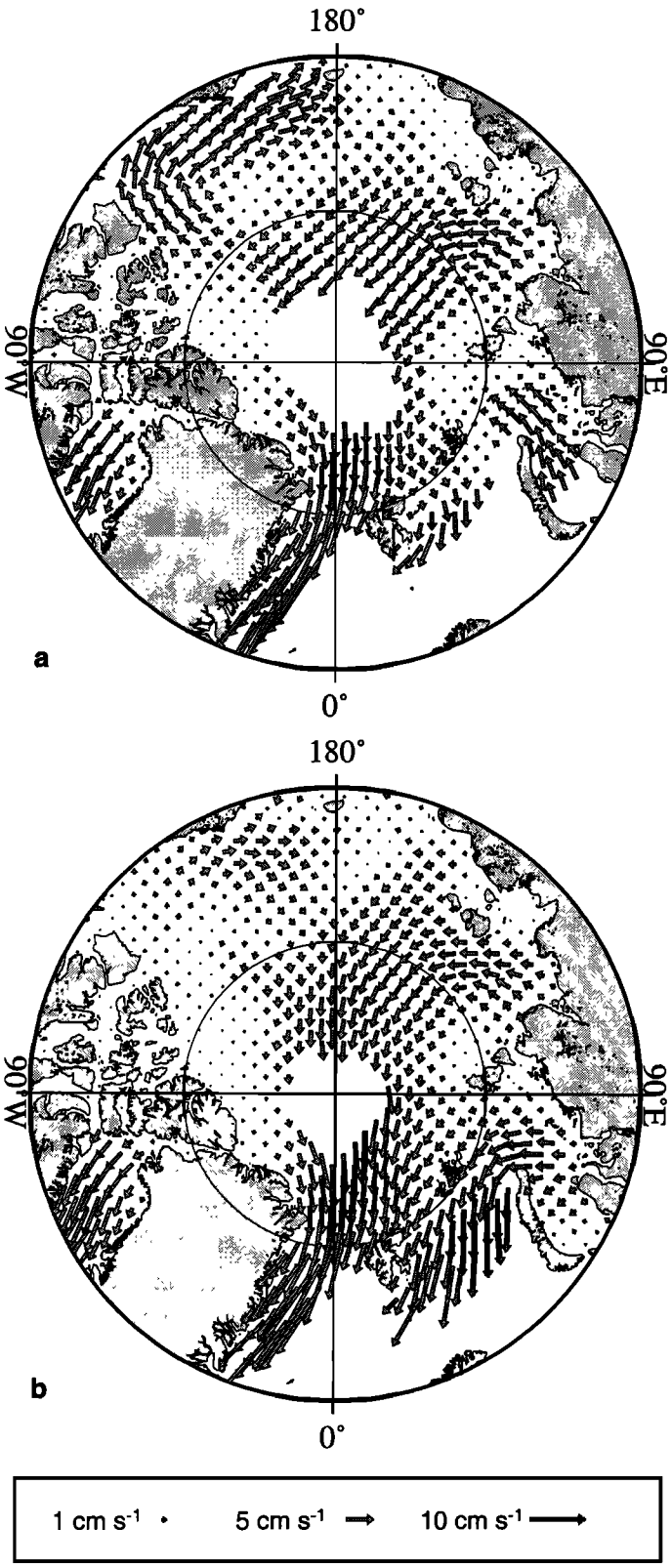

Figure 5. (a) Mean ice drift velocity between October 1987 and March 1988 retrieved from SSM/I data based on 141 single-drift calculations. Vectors are only shown for more than 60 individual values. (b) Mean ice drift velocity between October 1992 and March 1993 retrieved from SSM/I data based on 180 single-drift calculations. Vectors are only shown for more than 90 individual values.

the annual cycle in the sea level pressure field over the Arctic Ocean, pronounced interannual variations may occur that are also reflected in the ice drift. Recently, *Proshutinsky and Johnson* [1997] have classified the circulation of the wind-driven Arctic Ocean into two regimes, namely, one with a strong and the other with a weak Beaufort Gyre. Our 1987-1988 and 1992-1993 patterns reflect both of their circulation states. This concept is supported by the corresponding mean atmospheric sea level pressure fields displayed in Figure 7. In winter 1987-1988 a well-developed high-pressure system induces the anticyclonic ice drift in the Beaufort Sea. In 1992-1993 only a weak anticyclone exists over the Beaufort Sea, while a cyclonic flow dominates most of the Arctic Ocean and its adjacent shelf seas.

4.1. Local Variability

Some insight into the local variability of the ice flow can be gained from data analysis at the six different positions shown in Figure 8 for winter 1992-1993. The less complete data of 1987-1988 will not be considered here in depth since they are less reliable. Drift speed and direction distributions are displayed in Figure 9 as histograms and polar histograms (wind rose diagram), which show the distribution of the drift direction (in compass coordinates) weighted by their velocity values. Rather steady conditions prevail at Fram Strait (position A) and in the Arctic Ocean north of Fram Strait (positions B and C). The latter document convergence of the Transpolar drift on its approach into Fram Strait, so that the transport of sea ice is effectively concentrated toward the Fram Strait. The mean velocity of 0.1 m s^{-1} at position A is ~25% larger in 1992-1993 than in 1987-1988. This results in a higher ice transport across Fram Strait in 1992-1993 that is primaly fed by an increased contribution from the area north of Greenland passing position B.

The direction of the ice motion in the Laptev Sea and in the Canadian Basin varies to a much larger extent than in the European sector of the Arctic Ocean. The ice export from the Laptev Sea (position D) with a mean velocity of 0.07 m s^{-1} is similar in both periods, confirming that the Laptev Sea generally forms an important source region for the transpolar sea ice drift. At locations E and F in the area between Chukchi Sea and the Canadian Basin the drift directions vary considerably in 1992-1993 in contrast to 1987-1988 with the pronounced anticyclonic circulation of the Beaufort Gyre.

4.2. Mean Meridional Velocity at 81°N Latitude

The 81°N latitude circle more or less separates the Arctic Ocean from the shelf seas. Thus the mean meridional velocity component at 81°N (Figure 10) indicates the area transport of sea ice across the boundary of the Arctic Ocean. Southward ice transport is concentrated

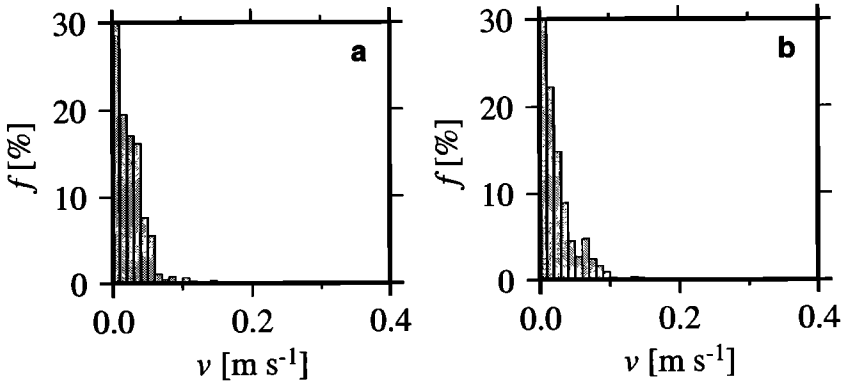

Figure 6. Histogram of the mean absolute ice drift velocities: (a) October 1987 to March 1988, and (b) October 1992 to March 1993.

on the sector between 20°W and 60°E longitude (Fram Strait and Barents Sea), while the advection is northward in all other sectors. As expected, the main export occurs through Fram Strait because of a narrow core of well-pronounced maximum velocities. In a first estimation the ice transport along 81°N into the Barents Sea is approximately of the same order as the ice import from the Kara Sea into the central Arctic Basin. The velocity profile of the Laptev Sea region is part of a clear regional trend with a minimum in the west and increasing velocities to the east. The velocity reaches its maximum in the East Siberian Sea and decreases in the areas of the Chukchi Sea and the Beaufort Sea from west to east. In the East Siberian Sea and the Laptev Sea the mean ice drift has a nearly northward direction, so that the frequent appearances of coastal polynyas during winter favor a high rate of ice production in these shelf areas.

4.3. Area Ice Flux

The area ice flux ($km^2\ s^{-1}$) is retrievable from the mean velocity components weighted by the spatial dimension of the ice drift. The product of the area flux and the ice thickness in meters leads to a volume flux in Sverdrup ($1\ Sv = 10^6\ m^3\ s^{-1}$). Since there were no sufficient ice thickness data available, our considerations were restricted to the area ice flux. The derived mean area fluxes from October 1992 to March 1993 are portrayed in Figure 11. A large net ice export from the shelf regions originates in the Kara Sea of 0.02 $km^2\ s^{-1}$ (north: 0.006 $km^2\ s^{-1}$; west: 0.014 $km^2\ s^{-1}$) and in the Laptev Sea of 0.015 $km^2\ s^{-1}$ (north: 0.008 $km^2\ s^{-1}$; east: 0.007 $km^2\ s^{-1}$). While the net ice flow from the Laptev Sea is toward the north and to the east, the transport from the Kara Sea is primarily directed to the west into the Barents Sea, very much in contrast to 1987-1988 where the ice flux was nearly zero, as shown in Figure 5. The meridional gradient at 80°N between Franz Josef Land and Severnaya Zemlya controls the strong ice export from the Kara Sea into the Barents Sea and the central Arctic Ocean, which has a corresponding distribution in the mean pressure data (Figure 7). Similar results have already been reported by *Vinje* [1987]. The Barents Sea appears in our analysis as a net ice sink area in general, which is confirmed by earlier investigations [*Aukrust and Oberhuber,* 1995; *Emery et al.,* 1997; *Pfirman et al.,* 1997]. Here it could be assumed that the prominent part of the imported ice will melt during the warmer season. In the winter 1992-1993 the mean net ice area import into the Barents Sea amounts to 0.023 $km^2\ s^{-1}$ with the largest amount coming from the Kara Sea. The estimation of the Fram Strait ice export is in good agreement with earlier export values calculated from AVHRR-based drift data [*Martin and Wadhams,* 1999]. The ice production (net ice outflow) of all areas and the ice export through Fram Strait and the Barents Sea are nearly balanced with 0.003 $km^2\ s^{-1}$ in 1992-1993. However, it is very likely that the ice exported into the Greenland and Barents Seas is distinctly thicker than the imported young ice from the other shelf seas. Therefore one must assume that the Arctic Ocean is a significant net source of sea ice on the annual average.

In the Fram Strait, ice thickness measurements have been made for several years using upward looking sonars mounted on oceanographic moorings [*Kvambekk and Vinje,* 1992; *Løyning and Nordlund,* 1995]. Taking from these data the corresponding monthly mean ice thickness, we arrive at a volume flux of 0.12 Sv (October 1992 to January 1993) across Fram Strait with a maximum of 0.15 Sv during January. *Vinje and Finnekåsa* [1986] also found a maximum ice flux for January. Their mean annual fluxes ranged between 0.12 and 0.23 Sv for the period 1976-1984 on the basis of a slightly larger mean ice thickness. Experiments with numerical large-scale sea ice models cover a wide range of ice fluxes across Fram Strait. *Harder et al.* [1998] have derived a mean volume flux of 0.12 Sv (October-March) with relative maxima in late autumn and in early spring. *Aukrust*

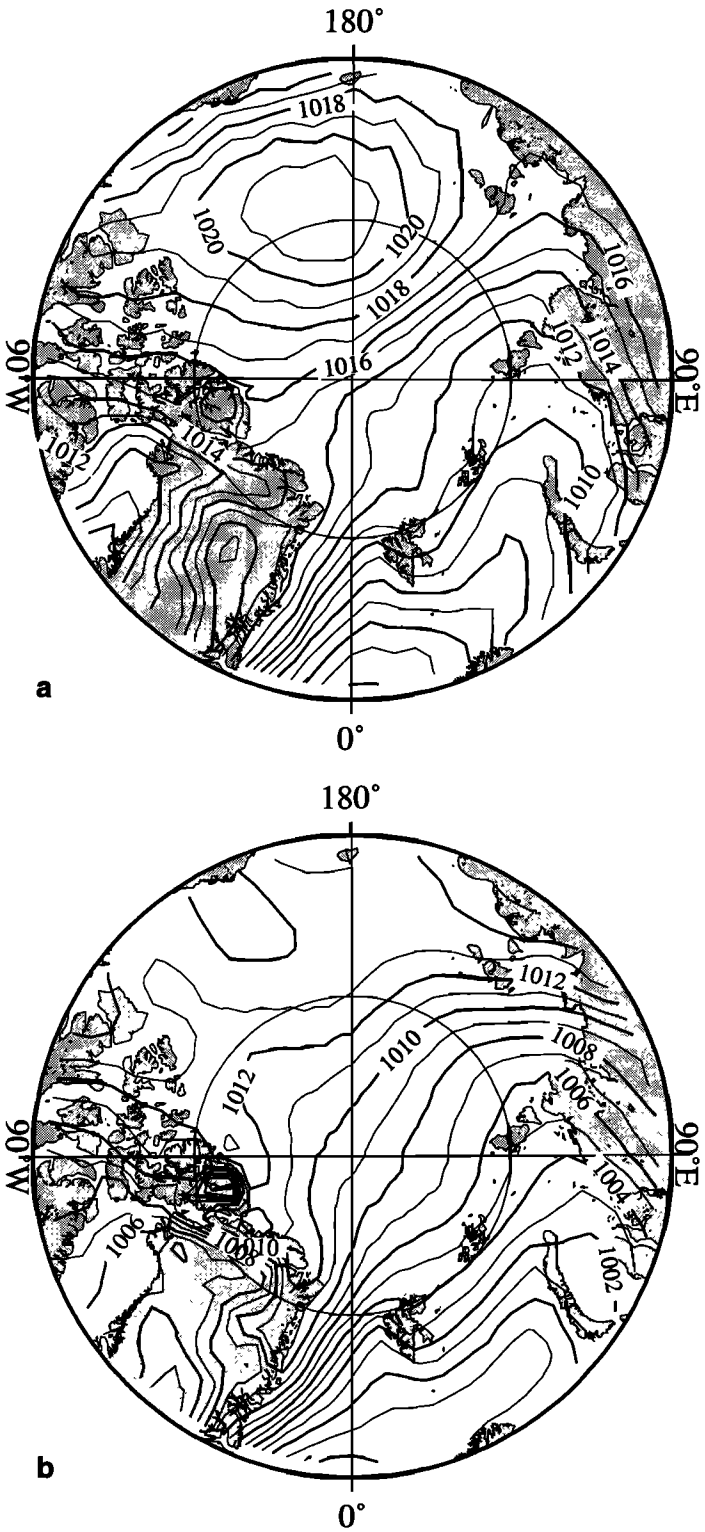

Figure 7. (a) Mean sea level pressure between October 1987 and March 1988. (b) Mean sea level pressure between October 1992 and March 1993.

and Oberhuber [1995] derived a maximum ice flux in March-April with a similar annual mean of 0.122 Sv. *Häkkinen* [1995] has computed a significantly smaller annual ice flux of 0.06 Sv. A satisfactory test of the various model results that might be best achieved for the Fram Strait region requires the extension of the analysis of the ice flow fields through at least a decade to cover the full scale of natural variability.

5. Conclusion

Our investigation has shown that the 85.5 GHz data of the SSM/I contain retrievable and reliable quantitative information on the sea ice drift in the Arctic. With the exception of the area around the North Pole a full area coverage of the drift vectors could be obtained. Local comparisons between the derived ice motion from microwave data and from drift buoys suggest a high degree of confidence of the SSM/I vectors. This conclusion is valid for the mean drift as well as for the temporal variability. The mean difference between the SSM/I drift data and the buoy data is $<\Delta v = 0.01$ m s^{-1}. The proposed time interval of 72 hours for the drift algorithm seems to be adequate to detect processes in a quasi-synoptical manner in all sea ice regions of the Arctic (see Figure 4). Therefore this investigation could not detect velocity variations on a time scale shorter than 72 hours as indicated in the 12 hour mean buoy data (Figures 1 and 2). It could be assumed that these fluctuations originated by local wind variations, ocean tides, and internal forces in the ice cover. Nevertheless, this part of the velocity spectrum has a more stochastical nature [*Colony and Thorndike,* 1985] and is therefore more important for opening and closing processes caused by lead development or in cases with convergent ice drift that results in deformation work and pressure ridge development in the ice. However, these effects could be neglected on compiling mean velocity fields covering weekly or monthly periods.

Our case studies refer to two configurations of the mean winter sea ice drift pattern due to differences of the atmospheric forcing conditions, which results in strong ice flux variations in the Kara Sea and in the Barents Sea. The monitoring of the interannual variability of the ice drift field makes possibile the weighting of variabilities, which could be caused by flow from different regions and therefore have different ice growth histories, in sea ice thickness measurements by upward looking sonar systems. The SSM/I drift data also have the potential to identify favorable locations for such thickness measurements, and to obtain a reliable total ice mass budget of the Artic Ocean.

The mean areas of ice production and ice melting have been confirmed, and the area ice fluxes have beeen determined with the aid of passive microwave satellite data. In contrast to the motion fields derived from drifting automatic buoys, the satellite method provides much better spatial mapping and resolves spatial gradients of velocity in more detail.

Data from the 85.5 GHz channel have been recorded by the DMSP satellites since 1987. With the aid of this data set the annual variability of the Arctic ice drift can

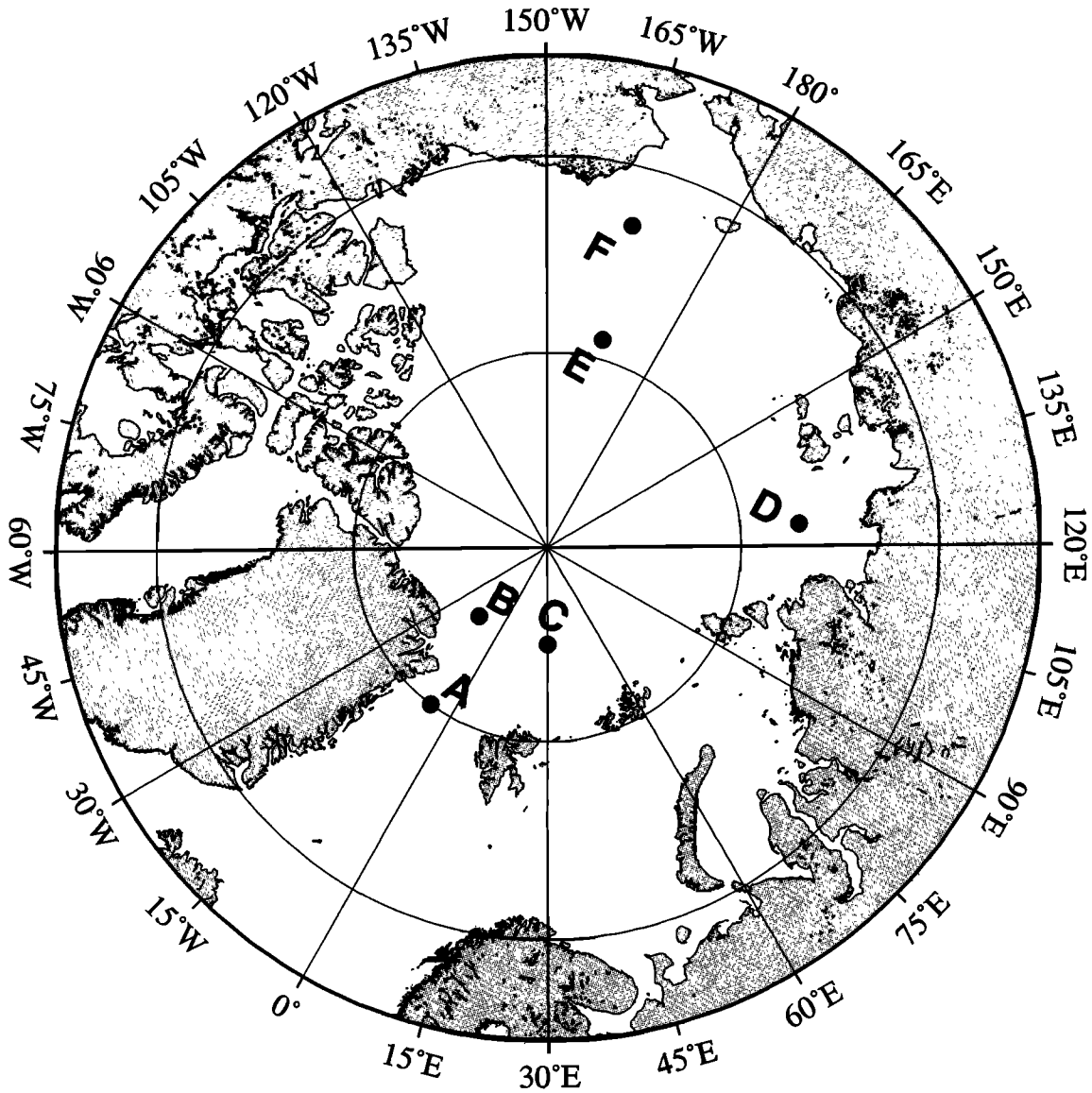

Figure 8. Positions of selected study locations.

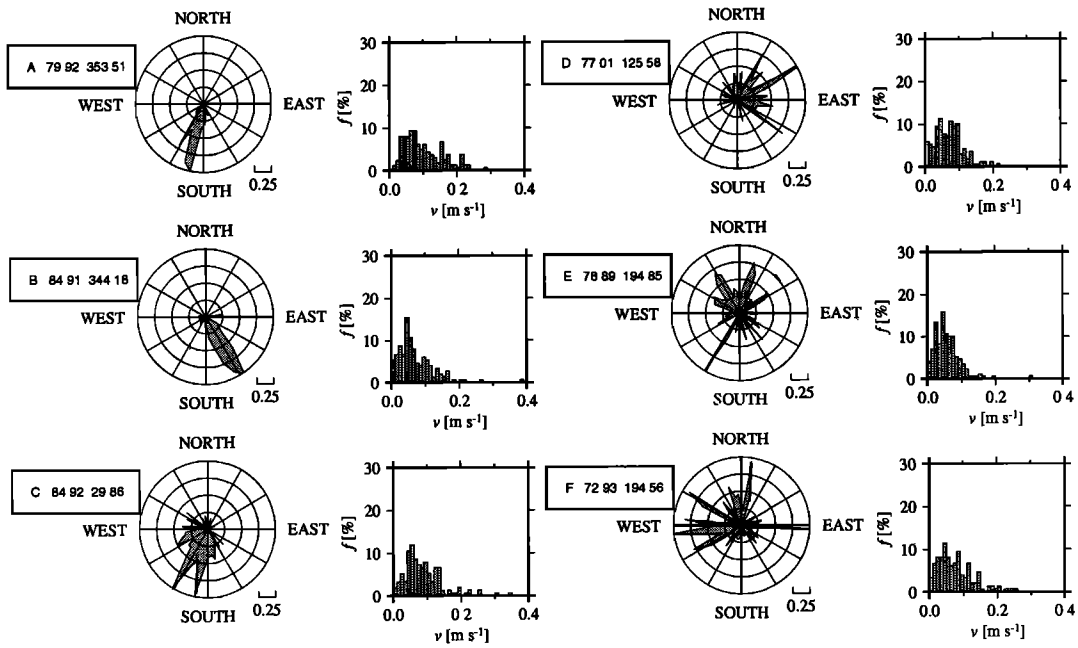

Figure 9. Normalized polar histograms (wind rose diagrams) and histograms of the ice drift velocity derived from SSM/I data at selected locations during the winter 1993-1994.

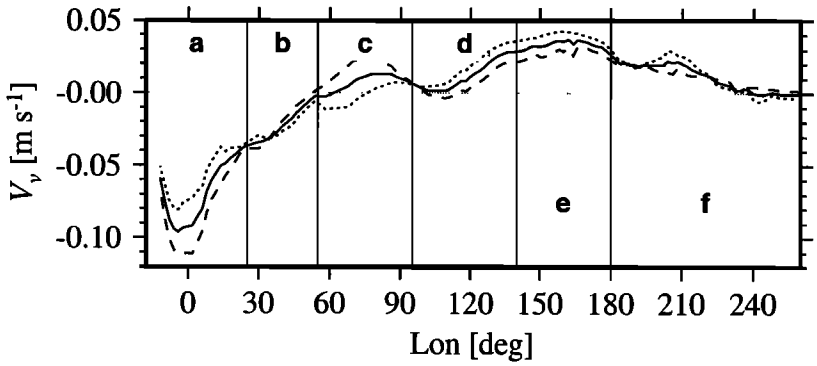

Figure 10. The mean meridional velocity component of sea ice drift along 81°N: (a) Fram Strait, (b) Barents Sea, (c) Kara Sea, (d) Laptev Sea, (e) East Siberian Sea, and (f) Chukchi Sea and Beaufort Sea. The solid line is the mean from October 1992 to March 1993; the dotted line is the mean from October to December 1992; and the dashed line is the mean from January to March 1993.

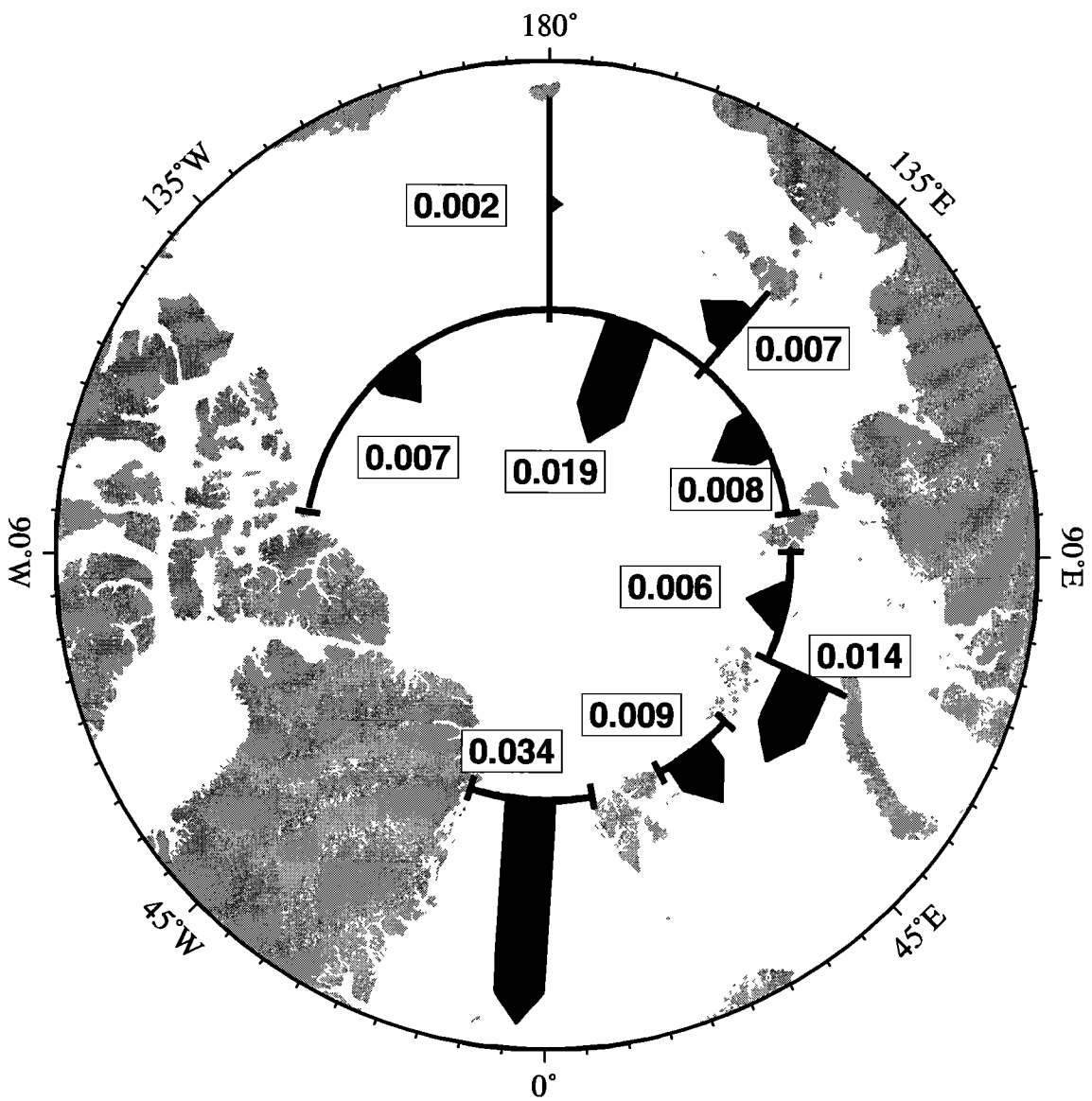

Figure 11. The Arctic mean area sea ice flux from October 1992 to March 1993 in km^2 s^{-1}.

now be reasonably derived for 10 years. Such a time series has been reliably used to test numerical sea ice models [*Kreyscher*, 1998] and could be used to monitor long-term changes of the Arctic sea ice.

Overall, the high quality of the SSM/I 85 GHz drift data results predominate the lack of a high spatial and temporal resolution. Therefore these data could provide a substantial contribution in studies focused more on interannual climate variability or on variability of the ice budget. The investigation of the short-term sea ice dynamics remains unsolved; also, these are a key process to getting more insight on the internal forces in the sea ice layer.

Acknowledgments. The daily SSM/I brightness temperature data were obtained from the EOSDIS NSIDC Distributed Active Archive Center (NSIDC DAAC), University of Colorado, Boulder. The buoy data are from the IABP provided by Ignatius Rigor, Applied Physics Laboratory, University of Washington. Atmospheric sea level pressure fields were derived from the ECMWF model analyses. This work was part of the ESOP-2 project supported by the MAST Programme of the European Union (MAS3-CT95-0015). This is contribution 1376 by the Alfred-Wegener-Institute for Polar and Marine Research.

References

Aagaard, K., J. H. Swift, and E. C. Carmack, Thermohaline circulation in the Arctic Mediterranean Seas, *J. Geophys. Res., 90*, 4833-4846, 1985.

Agnew, T. A., and H. Le, A more comprehensive view of the dynamics of Arctic sea ice as revealed through 85.5 GHz SSM/I imagery, *NSIDC Notes*, vol. 19, Nat. Snow and Ice Data Cent., Boulder, Colo., 1996.

Aukrust, T., and J. M. Oberhuber, Modeling the Greenland, Iceland, and Norwegian Seas with a coupled sea ice-mixed layer-isopycnal ocean model, *J. Geophys. Res., 100*, 4771-4789, 1995.

Barry, R. G., M. C. Serreze, J. A. Maslanik, and R. H. Preller, The Arctic sea ice-climate system: Observations and modeling, *Rev. Geophys., 31*, 397-422, 1993.

Björk, G., The relation between ice deformation, oceanic heat flux, and the ice thickness distribution in the Arctic Ocean, *J. Geophys. Res., 102*, 18,681-18,698, 1997.

Cavalieri, D. J., P. Gloersen, and W. J. Campbell, Determination of sea ice parameters with NIMBUS 7 SMMR, *J. Geophys. Res., 89*, 5355-5369, 1984.

Colony, R., and A. S. Thorndike, An estimate of the mean field of Arctic sea ice motion, *J. Geophys. Res., 89*, 10,623-10,629, 1984.

Colony, R., and A. S. Thorndike, Sea ice motion as a drunkard's walk, *J. Geophys. Res., 90*, 965-974, 1985.

Comiso, J. C., Characteristics of Arctic winter sea ice from satellite multispectral microwave observations, *J. Geophys. Res., 91*, 975-994, 1986.

Comiso, J. C., Arctic multiyear ice classification and summer ice cover using passive microwave satellite data, *J. Geophys. Res., 95*, 13,411-13,422, 1990.

Emery, W. J., C. W. Fowler, J. H. Hawkins, and R. H. Preller, Fram Strait satellite image-derived ice motion, *J. Geophys. Res., 96*, 4751-4768, 1991.

Emery, W. J., C. W. Fowler, and J. A. Maslanik, Satellite-derived maps of Arctic and Antarctic sea ice motion: 1988-1994, *Geophys. Res. Lett., 24*, 897-900, 1997.

Eppler, D. T., et al., Passive microwave signatures of sea ice, in *Microwave Remote Sensing of Sea Ice, Geophys. Monogr. Ser.*, vol. 68, edited by F. D. Carsey, pp. 47-71, AGU, Washington, D. C., 1992.

Fily, M., and A. Rothrock, Sea ice tracking by nested correlations, *IEEE Trans. Geosci. Remote Sens.*, 25, 570-580, 1987.

Gloersen, P., and D. J. Cavalieri, Reduction of weather effects in the calculation of sea ice concentration from microwave radiances, *J. Geophys. Res., 91*, 3913-3919, 1986.

Häkkinen, S., Simulated interannual variability of the Greenland Sea deep water formation and its connection to surface forcing, *J. Geophys. Res., 100*, 4761-4770, 1995.

Hallikainen, M. and D. P. Winebrenner, The physical basis for sea ice remote sensing, in *Microwave Remote Sensing of Sea Ice, Geophys. Monogr. Ser.*, vol. 68, edited by F. D. Carsey, pp. 29-46, AGU, Washington, D. C., 1992.

Harder, M., P. Lemke, and M. Hilmer, Simulation of sea ice transport through Fram Strait: Natural variability and sensitivity to forcing, *J. Geophys. Res., 103*, 5595-5606, 1998.

Hollinger, J. P., R. Lo, G. Poe, R. Savage, and J. Peirce, *Special Sensor Microwave/Imager User's Guide*, Naval Res. Lab., Washington, D. C., 1987.

Kamachi, M., Advective surface velocities derived from sequential images for rotational flow field: Limitations and applications of maximum cross-correlation method with rotational registration, *J. Geophys. Res., 94*, 18,227-18,233, 1989.

Kottmeier, C., et al., Wind, temperature and ice motion statistics in the Weddell Sea, in *International Programme for Antarctic Buoys/World Climate Research Programme*, World Meteorol. Org., Geneva, 1997.

Kreyscher, M., Dynamics of Arctic sea ice: Validation of different rheology schemes for the use in climate models, *Rep. Polar Res., 291*, Alfred Wegener Inst. for Polar and Mar. Res., Bremerhaven, Germany, 1998.

Kvambekk, Å. S., and T. Vinje, Ice draft recordings from upward looking sonars in the Fram Strait and Barents Sea in 1987/88 and 1990/91, *Papportserie 79*, Norsk Polarinst., Oslo, Norway, 1992.

Kwok, R., J. C. Curlander, R. McConnelli, and S. S. Pang, An ice-motion tracking system at the Alaska SAR Facility, *IEEE J. Oceanic Eng., 15*, 44-54, 1990.

Kwok, R., A. Schweiger, D. A. Rothrock, S. Pang, and C. Kottmeier, Sea ice motion from satellite passive microwave imagery assessed with ERS SAR and buoy motions, *J. Geophys. Res., 103*, 8191-8214, 1998.

Lemke, P., W. D. Hibler, G. Flato, M. Harder, and M. Kreyscher, On the improvement of sea-ice models for climate simulations: The Sea Ice Model Intercomparison Project, *Ann. Glaciol., 25*, 183-187, 1997.

Løyning, T. B., and N. Nordlund, Ice draft time series in the Fram Strait 1990-1994, in *Project Report from Task 3111 under ESOP, MAST II*, Norsk Polarinst., Oslo, Norway, 1995.

Martin, T., and P. Lemke, Sea ice drift and thickness in the East Greenland current, in *Nordic Seas*, pp. 135-138, Arct. Ocean Sci. Board and Sonderforschungsbereich "Proc. Relevant to Clim.", Hamburg, Germany, 1995.

Martin, T., and P. Wadhams, Sea-ice flux in the East Greenland current, *Deep Sea Res., Part II, 46*, 1063-1082, 1999.

Maslanik, J. A., Effects of weather on the retrieval of sea ice concentration and ice type from microwave data, *Int. J. Remote Sens., 13*, 37-54, 1992.

National Snow and Ice Data Center (NSIDC), DMSP SSM/I brightness temperature and sea ice concentration grids for the polar regions, in *User's Guide*, 2nd rev. ed., Dis-

tributed Active Arch. Cent., Univ. of Colo., Boulder, 1996.

Ninnis, R. M., W. J. Emery, and M. J. Collins, Automated extraction of pack ice motion from advanced very high resolution radiometer imagery, *J. Geophys. Res., 91*, 10,725-10,734, 1986.

Pfirman, S. L., R. Colony, D. Nürnberg, H. Eicken, and I. Rigor, Reconstructing the origin and trajectory of drifting Arctic sea ice, *J. Geophys. Res., 102*, 12,575-12,586, 1997.

Power, S. B., and L. A. Mysak, On the interannual variability of Arctic sea-level pressure and sea ice, *Atmos. Ocean, 30*, 551-577, 1992.

Proshutinsky, A. Y., and M. A. Johnson, Two circulation regimes of the wind-driven Arctic ocean, *J. Geophys. Res., 102*, 12,493-12,514 , 1997.

Rigor, I., and A. Heiberg, International Arctic buoy program data report, 1 January 1996 - 31 December 1996, *APL-UW TM 05-97*, Appl. Phys. Lab. Univ. of Wash., Seattle, 1997.

Serreze, M. C., R. G. Barry, and A. S. McLaren, Seasonal variations in sea ice motion and effects on sea ice concentration in the Canadian Basin, *J. Geophys. Res., 94*, 10,955-10,970, 1989.

Stern, H. L., D. A. Rothrock, and R. Kwok, Open water production in the Arctic sea ice: Satellite measurements and model parameterizations, *J. Geophys. Res., 100*, 20,601-20,612, 1995.

Thorndike, A. S., and R. Colony, Sea ice motion in response to geostrophic winds, *J. Geophys. Res., 87*, 5845-5852, 1982.

Vinje, T. E., Dynamics and morphology of the Barents Sea ice fields, in *Port and Ocean Engineering Under Arctic Conditions*, edited by W. A. Sackinger and M. O. Jeffries, Geophys. Inst., Univ. of Alaska, Fairbanks, 1987.

Vinje, T. E. and Ø. Finnekåsa, The ice transport through the Fram Strait, *Skr. Nor. Polarinst., 186*, 39 pp., 1986.

Vowinckel, E., and S. Orvig, Climate of the polar regions, in *World Survey of Climatology*, vol. 14, pp. 129-252, edited by S. Orvig, Elsevier Sci., New York, 1970.

Walters, J. M., C. Ruf, and C. T. Swift, A microwave radiometer weather-correction sea ice algorithm, *J. Geophys. Res., 92*, 6521-6534, 1987.

E. Augstein, Alfred-Wegener-Institute for Polar and Marine Research, Columbusstraße, D-27568 Bremerhaven, Germany. (eaugstein@awi-bremerhaven.de)

T. Martin, Institut für Meereskunde an der Universität Kiel, D-24105 Kiel, Germany. (tmartin@ifm.uni-kiel.de)

(Received January 26, 1998; revised September 8, 1999; accepted October 5, 1999.)